PHOTONICS Research

Controlled light distribution with coupled microresonator chains via Kerr symmetry breaking

Alekhya Ghosh,[1,2,†] Arghadeep Pal,[1,2,†] Lewis Hill,[1] Graeme N. Campbell,[1,3] Toby Bi,[1,2] Yaojing Zhang,[1] Abdullah Alabbadi,[1,2] Shuangyou Zhang,[1,2] and Pascal Del'Haye[1,2,*]

[1]Max Planck Institute for the Science of Light, D-91058 Erlangen, Germany
[2]Department of Physics, Friedrich Alexander University Erlangen-Nuremberg, D-91058 Erlangen, Germany
[3]Department of Physics, University of Strathclyde, Glasgow G4 0NG, UK
[†]These authors contributed equally to this work.
*Corresponding author: pascal.delhaye@mpl.mpg.de

Received 3 April 2024; revised 29 July 2024; accepted 29 July 2024; posted 30 July 2024 (Doc. ID 524823); published 1 October 2024

Within optical microresonators, the Kerr interaction of photons can lead to symmetry breaking of optical modes. In a ring resonator, this leads to the interesting effect that light preferably circulates in one direction or in one polarization state. Applications of this effect range from chip-integrated optical diodes to nonlinear polarization controllers and optical gyroscopes. In this work, we study Kerr-nonlinearity-induced symmetry breaking of light states in coupled resonator optical waveguides (CROWs). We discover, to our knowledge, a new type of controllable symmetry breaking that leads to emerging patterns of dark and bright resonators within the chains. Beyond stationary symmetry broken states, we observe Kerr-effect-induced homogeneous periodic oscillations, switching, and chaotic fluctuations of circulating powers in the resonators. Our findings are of interest for controlled multiplexing of light in photonic integrated circuits, neuromorphic computing, topological photonics, and soliton frequency combs in coupled resonators.

https://doi.org/10.1364/PRJ.524823

1. INTRODUCTION

When a system's physical or mathematical property remains unchanged under a certain transformation, it is said to possess symmetry. A sudden collapse of this symmetry is termed spontaneous symmetry breaking (SSB). SSB has answered pivotal questions in physics, ranging from the spontaneous breaking of gauge symmetry [1] to more contemporary models of continuous symmetry breaking in Rydberg arrays [2], the introduction of entanglement asymmetry [3], and SSB in quantum phase transitions [4]. The applications of SSB span over a large spectrum of physics [5–8].

Kerr ring resonators—Kerr here referring to cubic nonlinearity ($\chi^{(3)}$) in certain materials—have garnered interest for their capability to amass high light intensities within minuscule mode volumes, thereby enhancing the nonlinearity. These resonators have remarkable uses in optical frequency combs [9], telecommunications [10], spectroscopy [11], optical clocks [12], and sub-wavelength distance measurements [13]. Importantly, they also serve as experimental platforms for probing fundamental physical phenomena like SSB.

Within Kerr resonators, SSB has been studied extensively between counter-propagating optical fields during bidirectional pumping [14–21]. These systems have paved the way for designing optical isolators [22], circulators [23], and logic gates [24]. A second mechanism for realizing SSB originates from two co-propagating light fields with mutually orthogonal polarizations [25–29], which has led to the creation of polarization controllers [30], random number generators [31], and vectorial frequency combs [32]. Recent studies have unveiled SSB of solitons in Fabry–Perot resonators [33,34]. SSB via optomechanical effects has also been observed [35]. Recent innovations have expanded the two-field SSB phenomena to four-field SSB [36,37].

A myriad of other interesting solutions have been revealed by looking into slow-time responses, i.e., the evolutions of fields over many resonator round trips (t_r) in coupled cavities [38] and photonic dimers [35,37]. Fast-time (time scale of a single t_r) responses of coupled resonator optical waveguide (CROW) systems [39] and two-dimensional microresonator arrays [40,41] have also demonstrated a rich profusion of soliton dynamics. However, the slow-time response of CROW systems, rich in potential nonlinear effects, remains largely uncharted.

In this work, we conduct an in-depth study of two distinct CROW systems, and discuss the occurrence of concurrent SSBs

among different pairs of intra-resonator circulating intensities. In available literature demonstrating SSB, the symmetries between two opposite directions of propagation (i.e., clockwise and counter-clockwise) [14–18,42] or two mutually orthogonal circular polarizations [25–29] have been broken. However, in CROW systems, we report a different kind of SSB. In a linear CROW system without symmetry breaking, the circulating power in the resonators is mirror symmetric, meaning that the power in the first and last resonator is expected to be the same. The same applies to the second resonator and the second to last resonators as well as the other mirror symmetric resonator pairs in the chain. These equalities of powers or symmetries are broken in nonlinear CROW systems. The interplay of linear coupling and nonlinear interactions in our studied systems offers a vast parameter space to influence homogeneous responses. We demonstrate that varying input power levels leads the optical powers in the resonators to shift among different levels, exhibiting switch-like behaviors. This is promising for controllable distribution of light in photonic systems and realization of optical digital memories and computation systems. We also detect oscillations [20,43,44] that cause periodic interchanging of dominant field roles between distinct resonators and N-level chaotic oscillations in these systems. For silicon nitride resonators with Q-factors of about 10^8, all the nonlinear phenomena can be observed below input power of 150 mW. Precise on-chip microresonator fabrication methods [45] will make the proposed structures soon realizable on photonic chips, thus highlighting the pertinence of the work for guiding experiments in integrated photonics.

2. CROW SYSTEMS AND MODEL

In our study, we consider CROW systems, as illustrated in Fig. 1. The systems consist of several identical Kerr ring resonators are, forming a coupled resonator chain. Here, all the light fields supplied via the input ports are assumed to be identical, i.e., they have equal intensities, frequencies, polarizations,

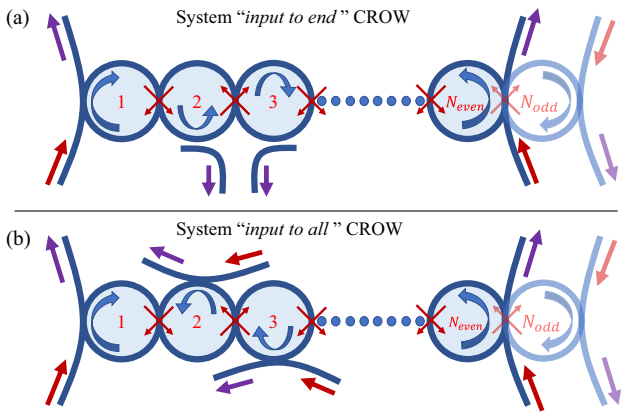

Fig. 1. CROW configurations. N identical Kerr ring resonators are linked in sequence. Input field directions ensure that each resonator's circulating field travels only in a singular direction. Note that systems with odd and even numbers of resonators require differing input directions for the end resonators; see faded resonators of the figure. (a) "Input to end" CROW: inputs are provided only to the end resonators. (b) "Input to all" CROW: inputs are connected to all resonators. Input (output) directions are shown by red (purple) arrows.

and phases. To begin with, we consider the situation when inputs are provided to only the first and last resonators in the chain. This configuration is depicted in Fig. 1(a). Afterwards, we also study the effects of facilitating inputs to all of the resonators [as shown in Fig. 1(b)]. Due to its more practical implementability, we first study the system with inputs only to the two resonators at the ends of the chain. The rich stationary state solutions and other homogeneous solutions of the system with more inputs are described later. Finally, in this study, we select the directions of input light fields that result in a system without counter-propagating fields.

Our modelling begins with normalized coupled Lugiato-Lefever equations (LLEs) [39,46]. For a system encompassing N coupled resonators (indexed as $n = 1, \ldots, N$ for $N \geq 2$), the equations manifest as

$$\frac{\partial \psi_n}{\partial \tau} = -(1 + i\zeta)\psi_n + i[(1 - \delta_{n,1})j\psi_{n-1} + (1 - \delta_{n,N})j\psi_{n+1}] + i|\psi_n|^2\psi_n + \alpha_n f, \quad (1)$$

where $\psi_n = \sqrt{2g_0/\kappa}A_n$ is the normalized optical field envelope in the nth resonator, within which A_n is the unnormalized field envelope, g_0 is the Kerr gain, and $\kappa = \kappa_l + \kappa_e$ is the total cavity losses, with internal losses κ_l and external losses κ_e. The normalized cavity detuning is given as $\zeta = 2\Delta/\kappa$, where the unnormalized cavity detuning is given as $\Delta = \omega_0 - \omega_{\text{res}}$ [the difference between the input laser frequency (ω_0) and the closest cavity resonance frequency (ω_{res})]. The terms within the brackets account for the inter-resonator couplings, where $\delta_{p,q}$ is the Kronecker delta function and $j = 2J/\kappa$ is the normalized inter-resonator coupling rate, with J being the unnormalized coupling rate. The normalized slow-time τ is defined as $\tau = 2t/\kappa$, where t is the unnormalized slow-time. Input to the resonators is given as $f = \sqrt{8\kappa_e g_0/\kappa^3}s_{\text{in}}e^{i\phi_{\text{in}}}$, where s_{in} and ϕ_{in} are respectively the input pump amplitude and the corresponding phase. In our simulations we assume ϕ_{in} to be constant and set it to $\phi_{\text{in}} = 0$ for convenience. The term $\alpha_n = 1$ when input is provided to the nth resonator and $\alpha_n = 0$ otherwise. The normalized intracavity intensity in the nth resonator is given by $\Psi_n = |\psi_n|^2$ and the input power by $F = |f|^2$. We have neglected dispersion in the systems. The second term (the term within the brackets) on the RHS of Eq. (1) describes the fact that all the resonators in the chain are coupled to the previous and the next resonator in the line except for the two end resonators, each of which is just connected to one adjacent resonator. The third term of Eq. (1) is the self-phase modulation term, which accounts for the nonlinear effect of a field on itself. The last term on the RHS of Eq. (1) represents input from outside the system. Since all the ring resonators in both cases are identical, parameters, such as the cavity detunings and the Kerr nonlinear gains, g_0, are the same for all resonators.

3. $N = 3$ CROW SYSTEMS

Our present analysis addresses CROWs with three or more resonators, i.e., $N \geq 3$. The homogeneous states of the systems are obtained by numerically evaluating Eq. (1) for a variety of initial conditions and over sufficient evolution times. The stationary states of the systems, which form a subset of the

homogeneous states, where the circulating fields remain unchanged over time, can be obtained by setting $\partial\psi_n/\partial\tau = 0$. For an $N = 3$ system, analytical solutions for the stationary states can be derived (see Appendix A for more details), but for $N > 3$ systems, obtaining analytical solutions is difficult. Since for $N \geq 3$, the two end resonators are connected to only one resonator while all other resonators in the CROW system are connected to two neighboring resonators, there is an inherent asymmetry in the system. The circulating field intensity in each resonator n is asymmetric to that of resonator m for $m \neq N - n + 1$. This asymmetry comes from the linear coupling terms of Eq. (1). Consequently, resonator n is symmetrical to only resonator $N - n + 1$ in terms of coupling arrangements. In other words, the field intensities are symmetric around the center of the chain.

Figure 2 shows different kinds of optical intensity distributions that can be observed in $N = 3$ CROW systems. In Fig. 2(a), it can be observed that for lower input powers, intracavity field intensities in the end resonators behave symmetrically, but the field intensity in the middle resonator is more than that of the individual end resonators. However, for a certain value of input power, the field intensities in the end resonators cross the field intensity in the middle resonator, and grow steadily after that, with the middle resonator's light intensity remaining almost constant. At the crossing point, there is a momentary occurrence of complete symmetry, where all three resonators have the same field intensities. Around the crossing point, the relative distribution of optical intensities between the middle resonator and the two end resonators can be tuned in a very controlled manner by changing the input power (discussed in Appendix B). Figure 2(b) reveals a spontaneous symmetry breaking of the circulating optical intensities in the end resonators. This adds to the various optical field distribution mechanisms that can be achieved in the CROW systems. It is important to note that the SSB depicted in Fig. 2(b) is a novel mechanism, quite different from the usual SSB observed in Kerr resonators [16,18,26,37]. The detailed description of the emergence of this SSB phenomenon is discussed in the next section. Following the trajectory of the field intensity in the middle resonator (in red) in Fig. 2(b), an interesting characteristic can be observed. The field intensity remains low for low input powers, jumps to a high value after a certain input power, and finally comes back to a low value in the SSB region. This effectively allows the system to be used as an all-optical switch with certain low and high cut-off powers. Apart from the stationary states, numerical simulations of Eq. (1) also reveal other homogeneous solutions, such as slow-time oscillations inside the resonators of the chain. Such Kerr-induced oscillations of the field intensities have been observed here with and without the occurrence of SSB in the system, as depicted in the upper and lower panels of Fig. 2(c), respectively. Oscillations of all field intensities are observed in the upper and lower panels of Fig. 2(d). In the upper panel, the middle resonator field intensity dominates over the end resonator field intensities, which always oscillate in phase. On the other hand, the lower panel shows a perfect periodic switching of the field intensities in the end resonators, where each of the three field intensities becomes dominant over the other two at certain instances. It is noteworthy that these homogeneous slow-time oscillations have much lower frequencies compared to the fast-time oscillations in

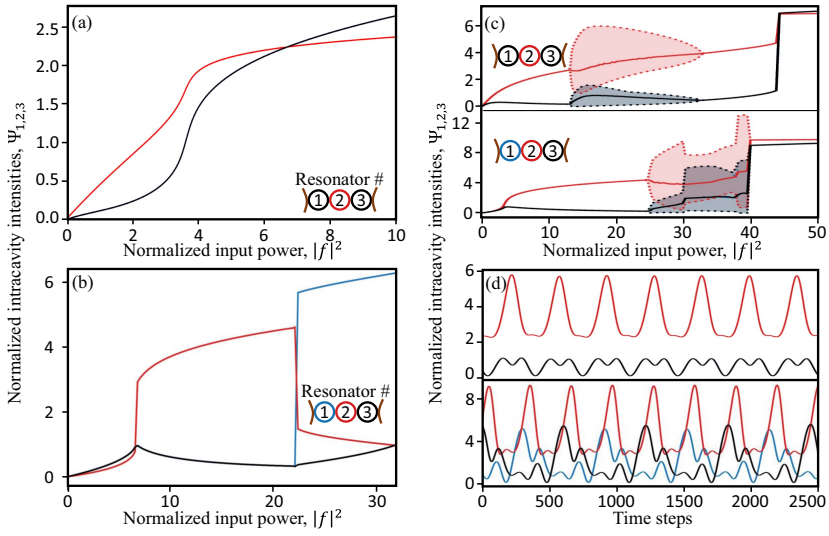

Fig. 2. Evolutions of optical intensities in $N = 3$ "input to end" CROW system. Panels (a)–(c) show the evolutions of the field intensities in different resonators as a function of input power. The field intensities in the end resonators are depicted in blue and black, whereas the field intensity in the middle resonator is depicted in red. For (a), $\zeta = 0.5, j = 1$. A field intensity crossing point appears in (a). Before the crossing point, the field intensity in the middle resonator is higher than the fields in the end resonators and beyond this point, the end resonator fields become more intense than the middle resonator field. Panel (b) depicts spontaneous symmetry breaking of the end resonator light field intensities for $\zeta = 5, j = 2$. Symmetry unbroken and symmetry broken oscillations are depicted in the upper ($\zeta = 3, j = 2$) and lower ($\zeta = 5, j = 2.5$) panels of (c), respectively. In this and all successive figures, the dotted lines stand for the positions of the maxima and the minima of the oscillations, and the shaded regions in between highlight the span of the oscillations. Upper and lower panels of (d) are examples of symmetry unbroken and complete symmetry broken oscillations, respectively. Used parameters: $|f|^2 = 22, \zeta = 3, j = 2$ [(d) upper panel], $|f|^2 = 37.79, \zeta = 5, j = 2.5$ [(d) lower panel]. Time step for integration is 0.005.

resonators, such as Turing oscillations. All of the observed phenomena pave the way for the $N = 3$ system to become an efficient option for optical field routing in integrated systems.

4. ANALYTICAL SOLUTION FOR $N = 3$ CROW SYSTEM

Input power, $|f|^2$, scans for an $N = 3$ CROW, when inputs are provided to only end resonators, are presented in Fig. 3. In Figs. 3(a) and 3(b) the analytical solutions to Eq. (1) are displayed. One may find details on the analytical solutions to Eq. (1) in Appendix A. Figures 3(a) and 3(b) reveal surprisingly rich and interesting dynamics for such a simple system. As mentioned earlier, for nonzero input powers, $\Psi_2 \neq \Psi_{1,3}$ due to coupling conditions. The difference in coupling causes persistent differences in the evolutions of the fields circulating the resonators, quite evident from the vastly different solution curves of Figs. 3(a) and 3(b). The analytical solutions of the end resonators, Fig. 3(b), reveal not one but two distinct sets of asymmetric solutions occurring for the end resonators. One set (blue) arises in a manner similar to that of previous studies—a pitchfork bifurcation emanating from the (red) symmetric solution line. The more surprising part is the second asymmetric solution set (green), which does not originate from a pitchfork bifurcation of the symmetric line. Indeed, it does not originate from the symmetric solution line at all. The green solution sets form entirely isolated solution "bubbles", an isolation seen most prominently in Fig. 3(a). Isolated sets of asymmetric solutions have not been seen in any past works, to our knowledge, with the exception of a significantly different setup with unbalanced input conditions [27]. A justified question to ask is the following: as interesting, perhaps, as the discovery of a novel SSB origin is, if these solutions are isolated, does this not imply that they are unreachable under experimental conditions—and hence entirely useless? We report that this is, highly surprisingly, not actually the case. Figures 3(c)–3(f) show, as a counterpart of the discussed analytical results, the results of the numerical integration of Eq. (1) via standard Runge-Kutta methods [Figs. 3(c) and 3(d) are extended versions of Fig. 2(b)]. In Figs. 3(c) and 3(d) the input power is stepwise increased following a suitable system relaxation time, while in Figs. 3(e) and 3(f) the input power is similarly stepwise decreased. Unlike the analytics, which provide the full solution sets, these scans predict the real-world behaviors and evolutions of the circulating fields under experimental conditions. From Fig. 3(d), we see that in the input-increasing-scan, just after $|f|^2 = 20$, the field intensities of the end resonators suddenly jump away from the red symmetric solution line and begin evolving, instead, along the green, isolated, asymmetric solution line. This is accompanied by a substantial drop in the middle resonator power, as seen in Fig. 3(c). The obvious question is, how. How does the system find the isolated set? The answer lies in the stability of Eq. (1). Performing a linear stability analysis, in Appendix C, we find that, at the point where the isolated asymmetric solutions occur, the symmetric solution line experiences a Hopf bifurcation (Appendix D) leading to system oscillations with wide-ranging intensity changes.

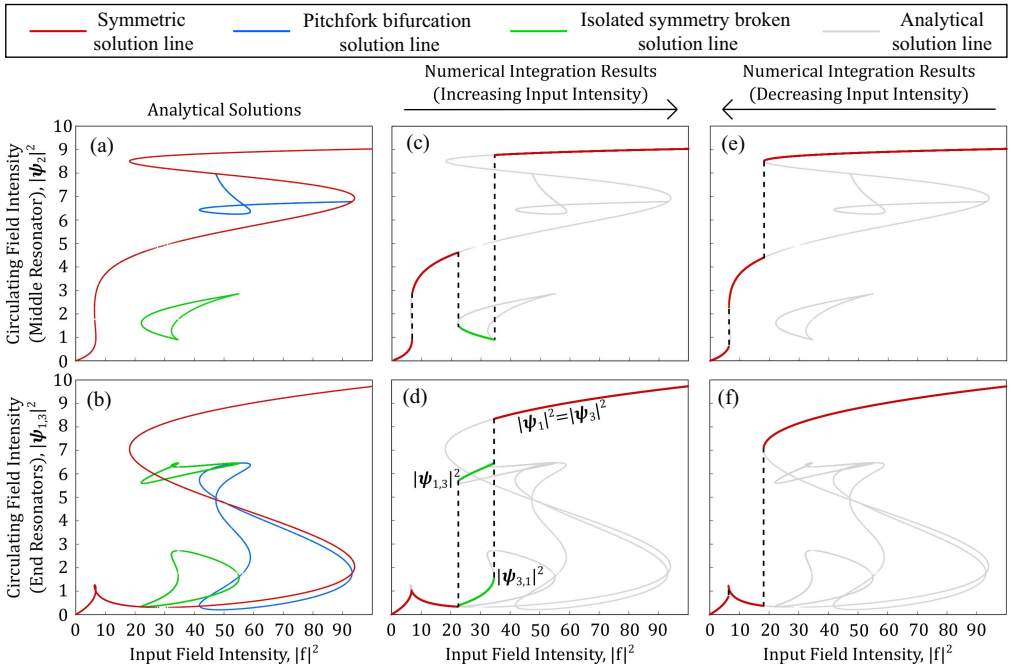

Fig. 3. Circulating field intensities, $\Psi_n(=|\psi_n|^2)$, against input power, $|f|^2$, for an $N = 3$ "input to end" CROW system. For detuning $\zeta = 5$ and inter-resonator coupling $j = 2$, we present in (a), (b) the analytical solutions to Eq. (1) for the fields circulating the middle Ψ_2 and end resonators $\Psi_{1,3}$, respectively. In panels (c), (d) and panels (e), (f), respectively, we display the results of numerical integrations of Eq. (1) for stepwise increasing and stepwise decreasing values of the input field intensity. In all panels, different "relationships" of solutions are colored accordingly for visual benefit; by this we mean that when fields $\Psi_{1,3}$ are on the green solution line, this means that Ψ_2 is also on its own respective green solution line. These results are discussed thoroughly in the main text, but we highlight the possibility of end-resonator-symmetric solutions (red) and two distinct end-resonator-symmetry-broken solutions (green and blue).

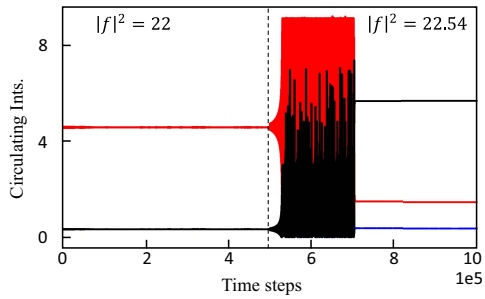

Fig. 4. Occurrence of SSB in $N = 3$ CROW system. The left side of the dashed line corresponds to a scan with an input power of 22.20, whereas the right side of the scan corresponds to a scan with an input power of 22.42. It can be seen that starting from a stable "black-blue symmetric" state, the system after the change in input power, goes to a "black-blue symmetry broken" state after a small oscillatory evolution. The origin of the oscillations can be described from the linear stability analysis presented in Appendices C and D. The blue and black lines represent the circulating field intensities in the end resonators, whereas the red line depicts the field in the middle resonator. The vertical dashed black line marks the point where the input power is increased. In each case, the detuning is five. Time step for integration is 0.005.

These oscillations allow for the system to eventually find, and settle on, attractive and stable, but isolated, asymmetric solutions. This process is shown in Fig. 4. As the increasing-input-scan continues further an optical bistability in the asymmetric states leads to the system losing stability once again and proceeds, this time, to settle on the stable upper branch of the original symmetric solution line. Owing to the strong stability of this upper branch, we find that a reverse scan in this case reveals none of the asymmetric solutions of the forward scan, only bistability jumps. Figure 3 has revealed that even for low values of N, Eq. (1) describes a system capable of extremely intricate dynamics.

5. CROW SYSTEMS WITH $N > 3$

To reveal the full potential of the CROW systems, we continue to study the homogeneous solutions in $N > 3$ systems. Figure 5 shows SSB phenomena occurring in the CROW systems with $N = 5$ and $N = 10$, with inputs provided only to the end resonators. In both systems, SSB bifurcations can be observed between different symmetric field pairs.

For lower input powers in the $N = 5$ system, $|\psi_1|^2 = |\psi_5|^2 \neq |\psi_2|^2 = |\psi_4|^2 \neq |\psi_3|^2$ and $|\psi_3|^2 \neq |\psi_1|^2$. In Fig. 5(a), where $\zeta = 3.5$ and $j = 1$, the field intensity in the middle resonator (in black, index 3) is suppressed greatly for all input power values. The intensities of the fields within the end resonators (indices 1 and 5—depicted in blue and cyan) and the set of resonators coupled to the end resonators (indices 2 and 4—depicted in red and green) display spontaneous symmetry

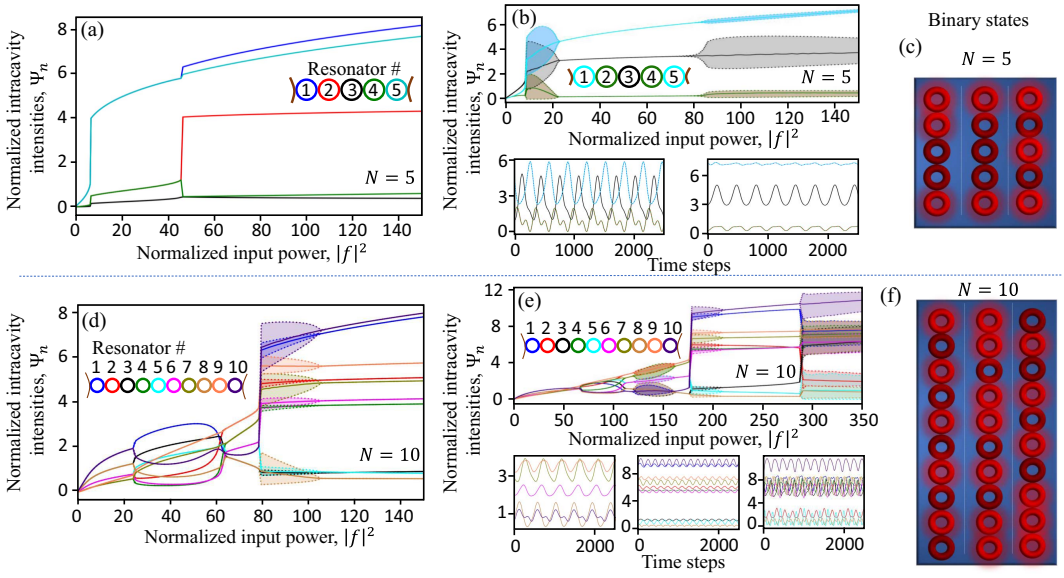

Fig. 5. Evolutions of optical intensities in (a)–(c) $N = 5$ and (d)–(f) $N = 10$ "input to end" CROW systems. Panel (a) and (b)-upper panel show the evolutions of the field intensities in different resonators as a function of input power. The end resonator field intensities are depicted in cyan and blue. In (a), the end resonator field intensities and the neighboring resonator's field intensities (depicted in red and green) display spontaneous symmetry breakings. In (b), the field intensities within coupling-wise symmetric resonators always remain symmetric and they display oscillations. Overlapping (lower-left panel) and non-overlapping (lower-right panel) oscillations are observed. In (c), we demonstrate three of the possible light intensity distribution conditions in the resonators with bright-red (dark-red) referring to bright (dark) resonators (left configuration: $\zeta = 3.62$, $J = 1$, $|f|^2 = 59.18$; middle configuration: $\zeta = 3.62, J = 1$, $|f|^2 = 37.88$; and right configuration: $\zeta = 3, J = 2$, $|f|^2 = 112.99$). Input power scans for $N = 10$ CROW systems are depicted in (d) and (e)-upper panel. All the symmetric field pairs undergo SSBs (in intensity) in (d) and upper panel of (e), followed by bistability jumps and symmetry broken oscillations. Moreover, symmetry unbroken oscillations are observed in the upper panel of (e). In the lower panel of (e), three examples of oscillations of field intensities in time are depicted from the different oscillatory regions as shown in the corresponding upper panel. Panel (f) presents three possible light distribution conditions (left configuration: $\zeta = 1.5$, $J = 4$, $|f|^2 = 37.88$; middle configuration: $\zeta = 1$, $J = 6$, $|f|^2 = 270.67$; and right configuration: $\zeta = 1$, $J = 6$, $|f|^2 = 88.38$). Used parameters: (a) $\zeta = 3.62$ and $j = 1$, (b) $\zeta = 3$ and $j = 2$, (d) $\zeta = 1.5$ and $j = 4$, and (e) $\zeta = 1$ and $j = 6$. Time step for integration is 0.005.

breakings. The system also shows bistability jumps. In the upper panel of Fig. 5(b), we can observe two isolated regions with symmetry unbroken oscillations in the system. The lower panel shows oscillations of circulating field intensities in time corresponding to the two different regions. Figure 5(c) depicts some of the possible steady state light field intensity distributions among different resonators for the $N = 5$ CROW system. Here, the state of a resonator is assumed to be bright if the circulating field intensity within the resonator is more than the average of all the resonator's field intensities in the respective CROW arrangement for a particular combination of system parameters and input powers.

Figures 5(d) and 5(e) depict the input power scans of the $N = 10$ system for two different sets of parameters. In Fig. 5(d), independent SSBs of all field intensities within resonators with symmetric coupling conditions are observed, with SSB bubbles crossing each other. The initial SSB region is followed by a symmetry restored region, which then is followed by regions of oscillating full asymmetric solutions, and subsequently non-oscillating full asymmetric solutions. Figure 5(e) depicts SSB of all coupling-wise symmetric pairs, symmetry restored regions with and without oscillations, and bistability jumps of the circulating field intensities leading to a second region of full asymmetry. This full asymmetric region also displays oscillations for certain ranges of input powers with and without overlaps. The lower panels of Fig. 5(e) show examples of field intensity oscillations in time corresponding to three different oscillatory regions. For CROW systems with an odd number of resonators, we observe $(N - 1)/2$ symmetry broken field pairs, since the middle resonator is not symmetric to any other resonator. However, for CROW systems with an even number of resonators, there are $N/2$ symmetric pairs at low power; therefore, we can observe up to $N/2$ symmetry broken field pairs.

Figure 5(f) shows some of the possible bright-dark conditions achievable in $N = 10$ CROW systems. These demonstrate the power distribution capabilities of the CROW systems. Different arrangements of bright-dark resonators, achievable via tuning the input power, can be used as different binary states. Therefore, the system can be used as an optical analog-to-digital converter where an analog optical input is transformed into a digital binary bit-string and multi-bit logical operations can be performed on them. Moreover, in Ref. [39], the authors have discussed the possibilities of having different dynamical fast-time solutions in the systems. These solutions, e.g., solitons, depend on the interplay of the dispersion profiles and nonlinear gains in the systems. The power redistribution that can be achieved in CROW systems can significantly change the intensity-dependent nonlinear gains in the resonators, affecting the fast-time dynamics. Therefore, by exploiting the interactions of the Kerr effect and coupling between resonators one can gain control over the fast-time dynamics in these systems.

Motivated by the fact that a rich variety of SSBs can be observed in the CROW system, we performed input power-detuning scans for $N = 3$, 5, 10, 20 and the corresponding results are depicted in Fig. 6. All the scans are performed for increasing input power. The scans demonstrate different

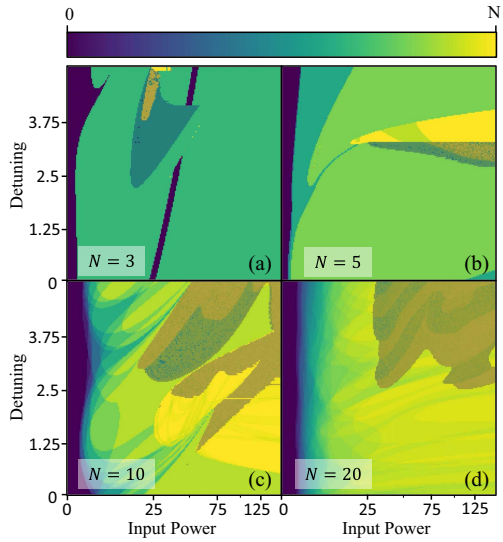

Fig. 6. Colormap of different symmetry breaking conditions as a function of input power and detuning for (a) $N = 3$, (b) $N = 5$, (c) $N = 10$, and (d) $N = 20$ "input to end" CROW systems. Purple regions stand for symmetry unbroken case and the yellow stands for completely asymmetric case. The colors in between (different shades of green) stand for different levels of symmetry breakings in the systems. The watershed portions with stripes in each panel display the regions of oscillations. In all cases, the scans are done from lower to higher input powers for certain detuning values. In other words, Eq. (1) is scanned for all detuning values starting from zero input power. For each input power, the initial values of the field amplitudes are selected to be the steady state value of the last step (smaller input power). The scans for all detunings are done in parallel. For the scans $j = 2$ (a), 1 (b), 3.5 (c), and 3 (d).

thresholded symmetry breaking conditions and oscillations of the circulating field intensities through different colored regions. Two fields are considered to be symmetric if the difference of their normalized intensities lies within an upper limit (here we choose 0.05). These scans can be used to allocate different amounts of homogeneous power in different resonators.

6. "INPUT TO ALL" CROW SYSTEMS

In this section of the paper, we aim to study the CROW configurations where all the resonators are provided with input fields. Since in these systems, all the resonators in the chain have access to input power [as shown in Fig. 7(a)], richer nonlinear effects are expected to be observed. The high degree of controllability of fields, due to inputs to all the resonators, makes this section important, especially for the experimentalists working on integrated coupled resonator systems.

For $N = 4$, the full asymmetry of circulating field intensities in different resonators is depicted in Fig. 7(b) for a wide range of input power values. The end resonator field intensities (in blue and green) initially remain symmetric and have less power than the middle resonators (indices 2 and 3, shown in black and red). With increasing input power, before the SSB region, a region of oscillation appears. The near-switching behaviors of the field intensities are depicted in the Appendix E. It is important to note that in the full asymmetric region, the

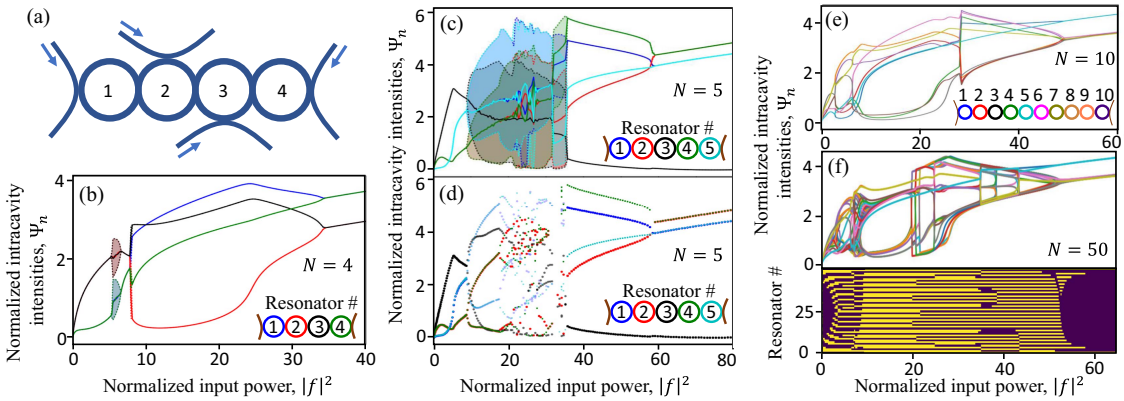

Fig. 7. Evolutions of optical intensities in "input to all" CROW systems for (b) $N = 4$, (c) $N = 5$, (e) $N = 10$, and (f) $N = 50$. Panel (a) depicts the schematic for a system with $N = 4$. Panel (b) presents the evolutions of the field intensities in an $N = 4$ CROW system with increasing input power for $\zeta = 1.5$ and $j = 1$. Oscillations, bistability jumps, and SSBs are observed sequentially in the system with increasing input power. Panel (c) shows the evolutions of the field intensities in an $N = 5$ CROW system with increasing input power for $\zeta = 2.5$ and $j = 2$. Panel (d) displays the Poincaré section plot of (c). In the region where dots of all colors look randomly scattered, chaos is observed. Panel (e) and the upper panel of (f) present evolutions of the field intensities for $N = 10$ ($\zeta = 1.5, j = 1$) and $N = 50$ ($\zeta = 1.5, j = 1$) CROW systems, respectively. In both cases, the fields within coupling-wise symmetric resonators break their symmetry with increasing input power; afterwards, they form two bunches, one at high power and the other one at low power. Thereafter in panel (e), by a bistability jump, the field intensities form two inverse bifurcation structures. In the upper panel of (f), several bistability jumps can be observed, where different field intensities group and regroup at different jumps. Finally, two inverse bifurcation structures form. The lower panel of (f) demonstrates the bright (yellow)-dark (purple) conditions of different resonators for different input powers.

crossing of the various fields' intensities leads to two very localized regions of three-level asymmetry. These particular crossings are intriguing since despite the different coupling conditions for the end and middle resonators, at some distinct input power levels one of the middle resonators becomes symmetric to one of the end resonators. The two SSB bubbles close by forming inverse bifurcation structures after a certain input power leading to two separated pairs of circulating field intensities. Here, each pair contains the fields within resonators that have symmetric coupling conditions, as observed for lower input powers. It can be observed that the dominance order of intensities of the pairs switches between before and after the SSB region.

With increasing N, more and more interesting nonlinear phenomena are observed. For an $N = 5$ system, Fig. 7(c) shows the input power-dependent redistribution of relative optical intensities among different resonators. The intensity of the middle resonator field (index = 3, in black) gradually decreases from being higher than any other fields at small input powers to being extremely suppressed after the complete symmetry breaking of all the fields. Figure 7(d) gives an insight into the oscillations in the system, which is portrayed via the Poincaré section plot, where the maxima and minima of the temporal oscillations of the respective field intensities are presented by dots for each input power. At the beginning of the oscillatory regime, the maxima and minima of the initially symmetric field intensities overlap completely. Therefore three regions of oscillations appear, the overlap regions of which gradually increase with input power. After the region of periodic oscillations, the system drives into the region of chaos with increasing input power, where all the field intensities oscillate asymmetrically. This symmetry broken chaotic oscillation region ends in symmetry broken stationary states. The full asymmetry closes with two inverse bifurcation structures. The SSB enforces high suppression of circulating power in the middle resonator, whereas the outer resonators always have higher circulating field intensities. A detailed overview of the oscillations for the $N = 5$ system is given in Appendix E.

For $N = 10$, as shown in Fig. 7(e), we again observe an SSB region; however, the SSB bubbles here twist and cross each other to provide different levels of symmetry breakings. At the end, following bistability jumps, the field intensities in the resonators form two inverse bifurcation structures, one by the fields within the end resonators, and one by all other fields. It is noteworthy that all the inner resonators at this point behave almost symmetrically. For $N = 50$, depicted in the upper panel of Fig. 6(f), SSB bubble crossings generate a much more complex scenario with many possible levels of SSB. However, a noticeable phenomenon in this case is the group formation of the field intensities within the SSB bubble, where two pairs of fields with little differences in intensities emerge. These intermediate pairs split up with multiple bistability jumps and a series of regroupings occurs. Finally, the field intensities merge into two symmetric pairs through two inverse bifurcation structures. For the first time, it has been observed that the field intensities jump between different levels of circulating power, forming a unique cage-like diagram in the regrouping section. Even if various resonators in the system have coupling-wise asymmetry, it is seen in both Figs. 7(e) and 7(f)-upper panel that after the inverse bifurcations only two bunches sustain, one by the fields within the end resonators, and the other one by all other fields. All the inner resonators at this point behave almost symmetrically. These SSB-induced intra-cavity field distributions in coupled resonator systems are not only

intriguing for generating multi-logic levels with higher functionalities in all-optical devices but also give an idea for observing various soliton dynamics at different input power levels.

In the lower panel of Fig. 7(f), we demonstrate the corresponding dark-bright conditions of different resonators as a function of input power. As mentioned earlier, a resonator is considered to be bright (shown in yellow) if the field intensity within that resonator is more than the average of all the field intensities of all the resonators. Otherwise, it is considered to be dark (shown in purple). The dark-bright condition plot shows that these configurations of CROW systems have great potential in all-optical computing. The input-output access to all the resonators makes it ideal for loading and unloading a bit-stream of data in a digital computing platform, with the ability to perform logical operations via the control of optical field distributions within the resonators.

It can be noted that due to the randomness associated with SSB, the dominance of circulating field amplitudes following symmetry breaking of each symmetric pair in a CROW is chosen randomly. For different simulation runs, the intracavity power plots can swap among the two resonators undergoing symmetry breaking. Similarly, in experiments, in a perfect symmetric case, after symmetry breaking, the dominance will be randomly assigned each time the system is pumped. This can be avoided, in order to achieve repeatability, by applying small input biases to the resonators. The resonators with the bias fields will always dominate in terms of circulating powers over their counterpart. However, this solution is not applicable for "input to end" CROW systems, where we cannot apply bias to all the resonators. In this case, relative detunings can be introduced between different resonators to achieve similar effects.

From an experimental outlook, we can consider silicon nitride resonators with radii 100 μm. If we assume the internal losses to be $\kappa_l = 50$ MHz and under the condition of critical coupling, i.e., $\kappa_e = 50$ MHz, one unit of normalized input power ($|f|^2 = 1$) corresponds to 0.109 mW.

7. DISCUSSION AND OUTLOOK

To summarize, a theoretical framework has been developed to examine different states of light in CROW systems. In CROW systems with inputs to the end resonators, we can observe a plethora of different symmetry breaking phenomena. The spontaneous symmetry breaking causes different light field intensities in different resonators. At low input powers, mirror symmetric pairs of resonators within the chain experience equal circulating powers. When the input power is increased, more complex light distributions within the resonator chain emerge, corresponding to multiple concurrent spontaneous symmetry breaking events. Symmetry broken oscillations are observed in $N = 3$, 5, 10 and 20 CROW systems for higher input powers and detunings. Periodic switchings between different pairs of field intensities are also observed. Due to the access of higher input powers to all resonators, richer nonlinear phenomena are observed in CROW systems with all resonators coupled to input waveguides. Extended regions of N-level SSBs and chaotic oscillations are observed in this type of CROW configuration.

Future research will address the dynamic behavior of optical fields in the resonators and the effects of asymmetry in different parameters on the homogeneous states of the systems. SSBs in other complex arrangements of microring resonators will also be addressed. The controllable distribution of light field intensities among different resonators could be a key feature for large-scale optical computing and light-field steering in integrated photonics. The combination of linear coupling between different resonators and optical nonlinearities in high-Q microresonators makes the CROW systems a promising candidate for integrated optical neural networks. CROW systems are also promising candidates for observing symmetry broken vector solitons with N different values of circulating intensities [32]. These can be useful for generating N distinct interconnected frequency combs, which would be very useful in neuromorphic computing, telecommunications, and especially in space technologies due to compactness. Together with the latest concepts of dispersion engineering [47–49] the studied nonlinear effects in this work will lead to a lot more interesting soliton dynamics.

APPENDIX A: THREE-RESONATOR CROW—ANALYTICAL SOLUTIONS

For a three-resonator CROW system the equations of motion take the form

$$\frac{\partial \psi_1}{\partial \tau} = -(1 + i\zeta_1)\psi_1 + ij\psi_2 + i|\psi_1|^2\psi_1 + \alpha_1 f, \quad \textbf{(A1a)}$$

$$\frac{\partial \psi_2}{\partial \tau} = -(1 + i\zeta_2)\psi_2 + i(j\psi_1 + j\psi_3) + i|\psi_2|^2\psi_2 + \alpha_2 f, \quad \textbf{(A1b)}$$

$$\frac{\partial \psi_3}{\partial \tau} = -(1 + i\zeta_3)\psi_3 + ij\psi_2 + i|\psi_3|^2\psi_3 + \alpha_3 f. \quad \textbf{(A1c)}$$

Here f is the input pump amplitude provided to the nth resonator ($n = 1$, 2, or 3) provided with detuning of ζ_n.

In steady state, all the equations become equal to zero. Solving the steady state equations for an "input to all" CROW system ($\alpha_1 = \alpha_2 = \alpha_3$), one can obtain

$$\Psi_1^3 - \Psi_3^3 + 2\zeta_3\Psi_3^2 - 2\zeta_1\Psi_1^2 + (1 + \zeta_1^2)\Psi_1 - (1 + \zeta_3^2)\Psi_3 = 0, \quad \textbf{(A2a)}$$

$$\Psi_2^3(C_3^2 + 1) + \Psi_2^2(2C_2C_3 + 2C_4) + \Psi_2(C_2^2 + C_4^2) = \Psi_1 C_5, \quad \textbf{(A2b)}$$

$$\left|-\left(1 - \frac{j^2}{D_1} - \frac{j^2}{D_3}\right) + i(\Psi_2 - \zeta_2)\right|^2 \Psi_2 = \left|1 - i\left(\frac{j}{D_1} + \frac{j}{D_3}\right)\right|^2 F, \quad \textbf{(A2c)}$$

where $\Psi_n = |\psi_n|^2$, $D_n = -(1 + i\zeta_n) + i\Psi_n$ (for $n = 1$,2 or 3), $C_1 = 1 - \zeta_2\zeta_3 - j\zeta_3$, $C_2 = C_1 + \zeta_2\Psi_3 + j\Psi_3$, $C_3 = \zeta_3 - \Psi_3$, $C_4 = -C_3 - \zeta_2 - j$, $C_5 = (1 + C_3(\Psi_1 - \zeta_1 - j) - j\zeta_1 + j\Psi_1)^2 + (\zeta_1 - \Psi_1 + C_3 + 2j)^2$, and $F = |f|^2$.

For an "input to end" CROW system, $\alpha_2 = 0$; therefore Eq. (A3) takes the form

$$\Psi_1^3 - \Psi_3^3 + 2\zeta_3\Psi_3^2 - 2\zeta_1\Psi_1^2 + (1+\zeta_1^2)\Psi_1 - (1+\zeta_3^2)\Psi_3 = 0, \quad \textbf{(A3a)}$$

$$\Psi_2^3 - 2\zeta_2\Psi_2^2 + \Psi_2(1+\zeta_2^2) = \Psi_1\left|j\left(\frac{D_3}{D_1}+1\right)\right|^2, \quad \textbf{(A3b)}$$

$$\left|D_2 + j^2\left(\frac{1}{D_1}+\frac{1}{D_3}\right)\right|^2\Psi_2 = \left|\left(\frac{j}{D_1}+\frac{j}{D_3}\right)\right|^2 F. \quad \textbf{(A3c)}$$

APPENDIX B: FIELD INTENSITY CROSSINGS FOR $N = 3$ "INPUT TO END" CROW SYSTEMS

For a symmetric CROW system, Eq. (A3b) takes the form

$$\Psi_2^3 - 2\zeta\Psi_2^2 + \Psi_2(1+\zeta^2) - 4j^2\Psi_1 = 0, \quad \textbf{(B1)}$$

where we have considered $\zeta_1 = \zeta_2 = \zeta_3 = \zeta$ and $D_1 = D_2 = D_3$. At the crossing points, $\Psi_1 = \Psi_2$,

$$\Psi_2 = \zeta \pm \sqrt{4j^2 - 1}. \quad \textbf{(B2)}$$

Further using Eq. (A3c), at the crossing points, one can obtain

$$F' = \left|\frac{-3 \pm i\sqrt{4j^2-1}}{2}\right|^2\left(\zeta \pm \sqrt{4j^2-1}\right). \quad \textbf{(B3)}$$

The conditions for having different numbers of crossings are mentioned in Table 1. Input power scans for different system parameters show different numbers of field crossing points in Fig. 8.

Table 1. Number of Field Intensity Crossing Points for $N = 3$

Number of Crossing Points	Conditions
0	$4j^2 < 1$
1	$4j^2 > 1$ and $\sqrt{4j^2-1} > \zeta$
2	$4j^2 > 1$ and $\sqrt{4j^2-1} < \zeta$

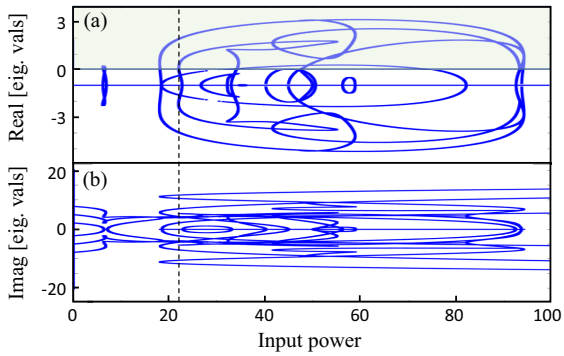

Fig. 9. SSB mechanism in $N = 3$ CROW system. Panels (a) and (b) show real and imaginary parts of eigenvalues of the Jacobian matrix of the system as given by Eq. (C2). The shaded region in panel (a) depicts the region where y-axis is above zero. When the real part of any of the eigenvalues enters the shaded region, the system becomes unstable. The dashed line (which is at the same place as the dashed line in Fig. 4 of the main manuscript) depicts the input power value for which the real part of one eigenvalue of the system goes above zero. The SSB between the circulating intensities in the end resonators occurs at this point.

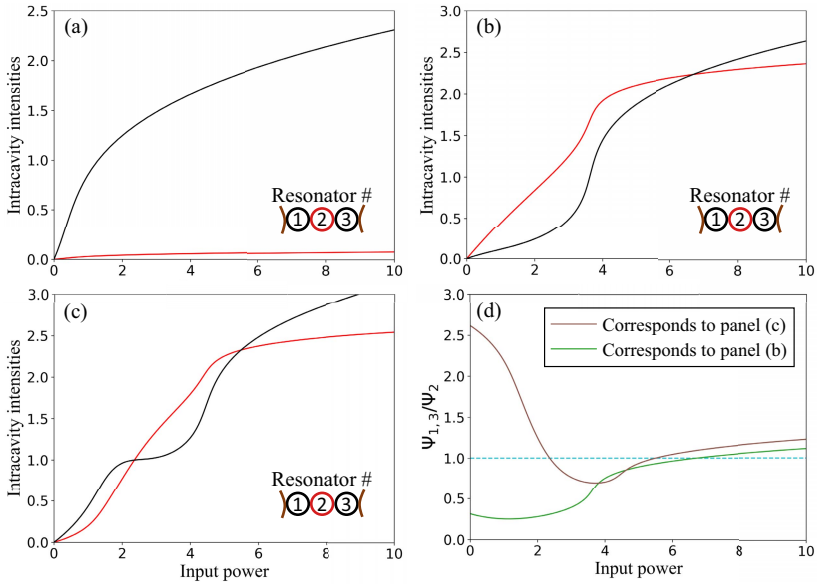

Fig. 8. Field intensity crossings for $N = 3$ "input to end" CROW systems. Panels (a)–(c) show input power scan of resonator light intensities for CROW systems with $N = 3$. In panel (a) the end resonator field intensities (shown in black) do not cross the field intensity in the middle resonator (shown in red). The middle resonator field intensity crosses end resonator field intensities once in panel (b) and twice in panel (c). Panel (d) shows the ratio of field intensities circulating in end resonators and middle resonator. Brown line shows the ratio for (b), and green line shows the ratio for (c). Panel (d) demonstrates the potential for relative power distributions among the resonators in $N = 3$ CROW systems. Used parameters: (a) $\zeta = 0.5$, $j = 0.1$, (b) $\zeta = 0.5$, $j = 1$, and (c) $\zeta = 1.66$, $j = 0.6$.

APPENDIX C: EIGENVALUE ANALYSIS FOR $N = 3$ "INPUT TO END" CROW SYSTEM

For the $N = 3$ CROW system, the normalized coupled LLEs take the form

$$\frac{\partial \psi_1}{\partial \tau} = -(1 + i\zeta)\psi_1 + ij\psi_2 + i|\psi_1|^2\psi_1 + f, \quad \textbf{(C1a)}$$

$$\frac{\partial \psi_2}{\partial \tau} = -(1 + i\zeta)\psi_2 + i(j\psi_1 + j\psi_3) + i|\psi_2|^2\psi_2, \quad \textbf{(C1b)}$$

$$\frac{\partial \psi_3}{\partial \tau} = -(1 + i\zeta)\psi_3 + ij\psi_2 + i|\psi_3|^2\psi_3 + f, \quad \textbf{(C1c)}$$

where ζ is the normalized detuning, j is the normalized coupling, ψ_n is the normalized field envelope in the nth resonator, and f is the input field amplitude. We define $\psi_n = \bar{\psi}_n + \delta\psi_n$, where $\bar{\psi}_n$ is the steady state value and $\delta\psi_n$ is the infinitesimal perturbation. Considering the complex conjugates of each field envelope, the evaluation equations for the perturbations can be written as $\dot{A} = \mathcal{J}A$, where $A = [\delta\psi_1, \delta\psi_1^*, \delta\psi_2, \delta\psi_2^*, \delta\psi_3, \delta\psi_3^*]^T$. The Jacobian matrix $\mathcal{J}$ can be written as

$$\mathcal{J} = \begin{bmatrix} \Delta_1 & i|\bar{\psi}_1|^2 & ij & 0 & 0 & 0 \\ -i|\bar{\psi}_1|^2 & \Delta_1^* & 0 & -ij & 0 & 0 \\ ij & 0 & \Delta_2 & i|\bar{\psi}_2|^2 & ij & 0 \\ 0 & -ij & -i|\bar{\psi}_2|^2 & \Delta_2^* & 0 & -ij \\ 0 & 0 & ij & 0 & \Delta_3 & i|\bar{\psi}_3|^2 \\ 0 & 0 & 0 & -ij & -i|\bar{\psi}_3|^2 & \Delta_3^*, \end{bmatrix}, \quad \textbf{(C2)}$$

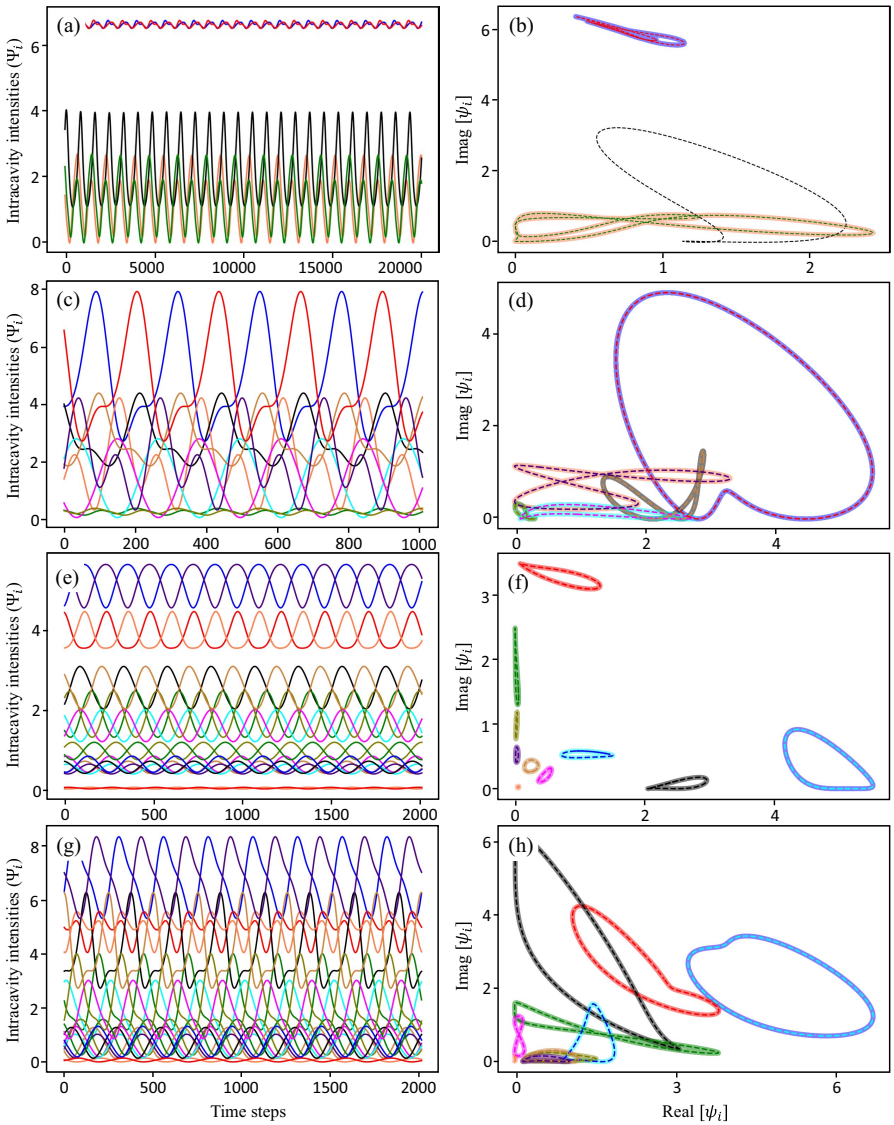

Fig. 10. Switchings in "input to end" CROW systems. Periodic switchings of the fields within coupling-wise symmetric resonators for (a), (b) $N = 5$, (c), (d) $N = 10$, (e)–(h) $N = 20$ are depicted. Perfect sinusoidal switchings (a), (c), (e), (g) are confirmed by the complete overlaps of the phase space plots (b), (d), (f), (h). Used parameters: (a) $|f|^2 = 108.34, \zeta = 3, j = 1$, (c) $|f|^2 = 39.18, \zeta = 4.2, j = 3.5$, (e) $|f|^2 = 67.53, \zeta = 4, j = 3$, (g) $|f|^2 = 120.05, \zeta = 4, j = 3$. Time step for integration is 0.005.

where $\Delta_n = -(1 + i\zeta - i2|\bar{\psi}_n|^2)$. When the real part of any of the eigenvalues of the matrix becomes positive, the system becomes unstable to perturbations.

APPENDIX D: ORIGIN OF THE NOVEL SYMMETRY BREAKING MECHANISM IN $N = 3$ CROW SYSTEM

In the main text, we have discussed the occurrence of a novel type of SSB in the $N = 3$ CROW system, where the system jumps from an initial symmetric state to an isolated set of asymmetric solutions via oscillations. The system starts to oscillate when the real part of any of its eigenvalues goes above zero. This is depicted in Fig. 9.

APPENDIX E: OSCILLATIONS IN CROW SYSTEMS

In the main paper, we have observed different types of oscillations in "input to end" CROW systems. We have also observed the perfect periodic switching in $N = 3$ CROW systems. In Figs. 10 and 11, we will observe different types of oscillations present in the $N > 3$ CROW systems with different input conditions.

APPENDIX F: EFFECTS OF FABRICATION-INDUCED ASYMMETRIES ON SSBS IN CROW

In the main paper, we have considered all the resonators forming the CROW systems to be identical. However, fabrication processes always introduce some uncertainties, which cause

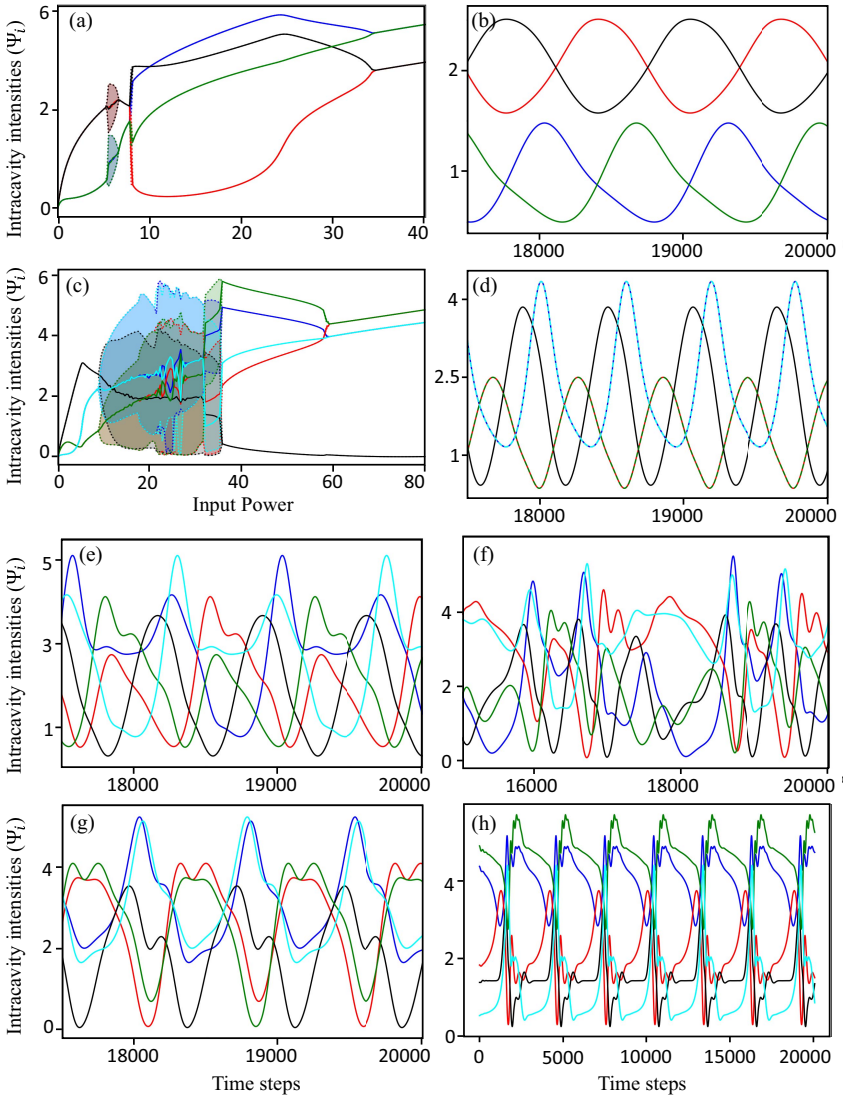

Fig. 11. Oscillations in "input to all" CROW systems. (a) Input power scan of resonator light intensities for CROW system with $N = 4$, $\zeta = 1.5$, and $j = 1$. (b) Evolutions of field intensities over time in the oscillatory region [shaded region in (a)] with $|f|^2 = 5.68$. (c) Input power scan of resonator light intensities for CROW system with $N = 5$, $\zeta = 2{,}5$, and $j = 2$. (d) and (e) show oscillations with maintained symmetry between fields within resonators with symmetric coupling conditions, whereas (f) shows switching oscillations between them. (g) depicts five-field chaos. (h) shows near-switching oscillations. $|f|^2 = 12.93$ (d), 20.20 (e), 24.44 (f), 29.09 (g), 34.14 (h). Time step for integration is 0.005.

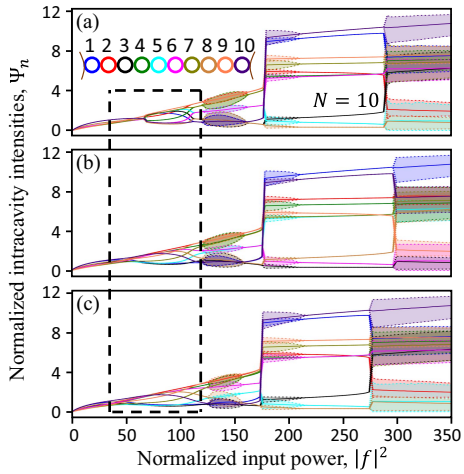

Fig. 12. Effects of fabrication-induced asymmetries in "input to end" CROW systems. Panels (a)–(c) show evolutions of circulating powers in different resonators with increasing input power in $N = 10$ "input to end" CROW systems. The detunings for the different resonators are assigned from a Gaussian distribution of mean 1 and standard deviation 0% (a), 5% (b), and 10% (c). Time step for integration is 0.005.

different resonators to have different optical path lengths of the optical modes confined in them. Therefore, there are inherent relative detunings between the resonances in different resonators. Such differences in detunings cause differences in coupled powers to the resonators with symmetrical coupling conditions under otherwise identical pumping conditions. Thus, in the absence of any initial symmetry between the coupling-wise symmetric resonators, we do not observe SSBs. Instead, we observe nonlinear enhancement of asymmetries of circulating power in them, which has been observed previously in single resonator systems [27] and coupled twin resonators [50]. In such a case, the dominating field following the SSB is not randomly chosen; instead, the resonator that has higher circulating optical power in the low input power regime always dominates over the other resonator having identical coupling conditions. In this section, we have analyzed the effects of introducing structural asymmetries among different resonators. We have introduced Gaussian noise to the detunings with standard deviations of 1%, 5%, and 10% of the mean detuning for the $N = 10$ "input to end" CROW system and presented the input power scan in Fig. 12. It can be observed that (inside the region enclosed by the dashed black box) the SSB bubbles for the "no-defect" case (standard deviation of detuning distribution, 0% of its mean value) are not present for increased structural asymmetries. However, Kerr-effect-induced enhancement of circulating power differences in the coupling-wise symmetric resonators can be observed. Apart from this region (black box), there is no significant qualitative change in the distribution of optical powers across different resonators.

Figure 13 focuses on the region within the black dashed box in Fig. 12. One can observe that with increasing Gaussian noise on the resonance frequency detunings of the resonators, the field profiles deviate from SSB profiles. However, even in systems with asymmetries, the differences of circulating optical intensities in resonators with identical coupling conditions are enhanced.

Moreover, it is possible to balance the inherent asymmetries between the resonators forming a CROW by all-optical ways [27]. In integrated systems, heating different resonators with integrated heaters [51] can help to overlap the resonance frequencies of the different resonators. One can also make the resonators highly coupled to each other, which broadens the resonances, ensuring spectral overlap [41].

Funding. Max-Planck-Gesellschaft; European Research Council (756966).

Acknowledgment. AG and AP acknowledge the support from the Max Planck School of Photonics. LH acknowledges funding provided by the SALTO funding scheme from the MPG and Centre National de la Recherche Scientifique

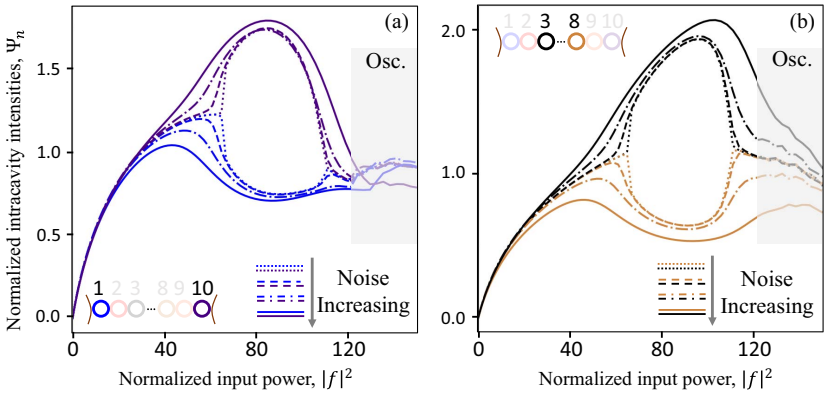

Fig. 13. Nonlinear enhancement of asymmetries in "input to end" CROW systems with nonidentical resonators. Evolutions of circulating powers in resonators (a) 1 and 10 and (b) 3 and 8 with increasing input power in $N = 10$ "input to end" CROW system are depicted. With increasing variations of inherent inter-resonator detuning, SSB is substituted by nonlinear enhancement of inter-resonator optical power difference. The detunings for the different resonators are assigned from a Gaussian distribution of mean 1 and standard deviation 0% (dotted lines), 1% (dashed lines), 5% (dashed-dotted lines), and 10% (solid lines) of its mean. Inter-resonator coupling is set to $j = 6$. Field intensities display oscillatory responses in the shaded regions. Time step for integration is 0.005.

(CNRS). The authors thank Prof. Gian-Luca Oppo for the fruitful discussions.

Author Contributions. PDH, AG, and LH defined the research project. AG performed the theoretical analysis with support from LH and AP. AP, AG, and LH completed the numerical simulations. AG, AP, LH, and PDH wrote the manuscript with the help of all other authors. PDH and LH supervised the project.

Disclosures. The authors declare no conflicts of interest.

Data Availability. Data underlying the results may be obtained from the authors upon reasonable request.

REFERENCES

1. J. Bernstein, "Spontaneous symmetry breaking, gauge theories, the Higgs mechanism and all that," Rev. Mod. Phys. **46**, 7–48 (1974).
2. C. Chen, G. Bornet, M. Bintz, *et al.*, "Continuous symmetry breaking in a two-dimensional Rydberg array," Nature **616**, 691–695 (2023).
3. F. Ares, S. Murciano, and P. Calabrese, "Entanglement asymmetry as a probe of symmetry breaking," Nat. Commun. **14**, 2036 (2023).
4. W. Ning, R.-H. Zheng, J.-H. Lü, *et al.*, "Experimental observation of spontaneous symmetry breaking in a quantum phase transition," Sci. China Phys. Mech. Astron. **67**, 220312 (2024).
5. H. Arodz, J. Dziarmaga, and W. Zurek, *Patterns of Symmetry Breaking*, Nato Science Series II (Springer Netherlands, 2011).
6. M. He, Y. Li, J. Cai, *et al.*, "Symmetry breaking in twisted double bilayer graphene," Nat. Phys. **17**, 26–30 (2021).
7. G. Barbillon, A. Ivanov, and A. K. Sarychev, "Applications of symmetry breaking in plasmonics," Symmetry **12**, 896 (2020).
8. Y. Lin, D. Wang, J. Hu, *et al.*, "Engineering symmetry-breaking nanocrescent arrays for nanolasing," Adv. Funct. Mater. **29**, 1904157 (2019).
9. P. Del'Haye, A. Schliesser, O. Arcizet, *et al.*, "Optical frequency comb generation from a monolithic microresonator," Nature **450**, 1214–1217 (2007).
10. J. N. Kemal, P. Marin-Palomo, M. Karpov, *et al.*, "Chip-based frequency combs for wavelength-division multiplexing applications," in *Optical Fiber Telecommunications VII* (Elsevier, 2020), pp. 51–102.
11. N. Picqué and T. W. Hänsch, "Frequency comb spectroscopy," Nat. Photonics **13**, 146–157 (2019).
12. S. B. Papp, K. Beha, P. Del'Haye, *et al.*, "Microresonator frequency comb optical clock," Optica **1**, 10–14 (2014).
13. H. Yan, A. Ghosh, A. Pal, *et al.*, "Real-time imaging of standing-wave patterns in microresonators," Proc. Natl. Acad. Sci. USA **121**, e2313981121 (2024).
14. A. Kaplan and P. Meystre, "Directionally asymmetrical bistability in a symmetrically pumped nonlinear ring interferometer," Opt. Commun. **40**, 229–232 (1982).
15. E. M. Wright, P. Meystre, W. J. Firth, *et al.*, "Theory of the nonlinear Sagnac effect in a fiber-optic gyroscope," Phys. Rev. A **32**, 2857–2863 (1985).
16. M. T. M. Woodley, J. M. Silver, L. Hill, *et al.*, "Universal symmetry-breaking dynamics for the Kerr interaction of counterpropagating light in dielectric ring resonators," Phys. Rev. A **98**, 053863 (2018).
17. L. Hill, G.-L. Oppo, M. T. M. Woodley, *et al.*, "Effects of self- and cross-phase modulation on the spontaneous symmetry breaking of light in ring resonators," Phys. Rev. A **101**, 013823 (2020).
18. L. Del Bino, J. M. Silver, S. L. Stebbings, *et al.*, "Symmetry breaking of counter-propagating light in a nonlinear resonator," Sci. Rep. **7**, 43142 (2017).
19. Q.-T. Cao, H. Wang, C.-H. Dong, *et al.*, "Experimental demonstration of spontaneous chirality in a nonlinear microresonator," Phys. Rev. Lett. **118**, 033901 (2017).
20. M. T. M. Woodley, L. Hill, L. Del Bino, *et al.*, "Self-switching Kerr oscillations of counterpropagating light in microresonators," Phys. Rev. Lett. **126**, 043901 (2021).
21. G. N. Campbell, S. Zhang, L. Del Bino, *et al.*, "Counterpropagating light in ring resonators: switching fronts, plateaus, and oscillations," Phys. Rev. A **106**, 043507 (2022).
22. A. D. White, G. H. Ahn, K. V. Gasse, *et al.*, "Integrated passive nonlinear optical isolators," Nat. Photonics **17**, 143–149 (2023).
23. L. D. Bino, J. M. Silver, M. T. M. Woodley, *et al.*, "Microresonator isolators and circulators based on the intrinsic nonreciprocity of the Kerr effect," Optica **5**, 279–282 (2018).
24. N. Moroney, L. D. Bino, M. T. M. Woodley, *et al.*, "Logic gates based on interaction of counterpropagating light in microresonators," J. Lightwave Technol. **38**, 1414–1419 (2020).
25. J. Geddes, J. Moloney, E. Wright, *et al.*, "Polarisation patterns in a nonlinear cavity," Opt. Commun. **111**, 623–631 (1994).
26. F. Copie, M. T. Woodley, L. Del Bino, *et al.*, "Interplay of polarization and time-reversal symmetry breaking in synchronously pumped ring resonators," Phys. Rev. Lett. **122**, 013905 (2019).
27. B. Garbin, J. Fatome, G.-L. Oppo, *et al.*, "Asymmetric balance in symmetry breaking," Phys. Rev. Res **2**, 023244 (2020).
28. T. Huang, H. Zheng, G. Xu, *et al.*, "Coexistence of nonlinear states with different polarizations in a Kerr resonator," Phys. Rev. A **109**, 013503 (2024).
29. J. Fatome, E. Lucas, B. Kibler, *et al.*, "Observation of polarization faticons in a fibre Kerr resonator," in *European Quantum Electronics Conference* (Optica Publishing Group, 2023), paper pd_2_7.
30. N. Moroney, L. Del Bino, S. Zhang, *et al.*, "A Kerr polarization controller," Nat. Commun. **13**, 398 (2022).
31. L. Quinn, G. Xu, Y. Xu, *et al.*, "Random number generation using spontaneous symmetry breaking in a Kerr resonator," Opt. Lett. **48**, 3741–3744 (2023).
32. G. Xu, A. U. Nielsen, B. Garbin, *et al.*, "Spontaneous symmetry breaking of dissipative optical solitons in a two-component Kerr resonator," Nat. Commun. **12**, 4023 (2021).
33. L. Hill, E.-M. Hirmer, G. Campbell, *et al.*, "Symmetry broken vectorial Kerr frequency combs from Fabry-Pérot resonators," Commun. Phys. **7**, 82 (2024).
34. G. N. Campbell, L. Hill, and P. Del'Haye, , *et al.*, "Dark temporal cavity soliton pairs in Fabry-Pérot resonators with normal dispersion and orthogonal polarizations," in *Conference on Lasers and Electro-Optics Europe & European Quantum Electronics Conference (CLEO/Europe-EQEC)* (2023) paper ef_p_3.
35. M.-A. Miri, E. Verhagen, and A. Alù, "Optomechanically induced spontaneous symmetry breaking," Phys. Rev. A **95**, 053822 (2017).
36. L. Hill, G.-L. Oppo, and P. Del'Haye, "Multi-stage spontaneous symmetry breaking of light in Kerr ring resonators," Commun. Phys. **6**, 208 (2023).
37. A. Ghosh, L. Hill, and G.-L. Oppo, , *et al.*, "Four-field symmetry breakings in twin-resonator photonic isomers," Phys. Rev. Res. **5**, L042012 (2023).
38. J. Mai, X. Huang, X. Guo, *et al.*, "Spontaneous symmetry breaking of coupled Fabry–Pérot nanocavities," Commun. Phys. **7**, 223 (2024).
39. A. Tusnin, A. Tikan, K. Komagata, *et al.*, "Nonlinear dynamics and Kerr frequency comb formation in lattices of coupled microresonators," Commun. Phys. **6**, 317 (2023).
40. S. Mittal, G. Moille, K. Srinivasan, *et al.*, "Topological frequency combs and nested temporal solitons," Nat. Phys. **17**, 1169–1176 (2021).
41. C. J. Flower, M. Jalali Mehrabad, L. Xu, *et al.*, "Observation of topological frequency combs," Science **384**, 1356–1361 (2024).
42. A. Ghosh, A. Pal, S. Zhang, *et al.*, "Phase symmetry breaking of counterpropagating light in microresonators for switches and logic gates," arXiv, arXiv:2407.16625 (2024).
43. R. D. D. Bitha, A. Giraldo, N. G. Broderick, *et al.*, "Bifurcation analysis of complex switching oscillations in a Kerr microring resonator," Phys. Rev. E **108**, 064204 (2023).

44. G. Xu, L. Hill, J. Fatome, *et al.*, "Breathing dynamics of symmetry-broken temporal cavity solitons in Kerr ring resonators," Opt. Lett. **47**, 1486–1489 (2022).
45. S. Zhang, T. Bi, I. Harder, *et al.*, "Low-temperature sputtered ultralow-loss silicon nitride for hybrid photonic integration," Laser Photonics Rev. **18**, 2300642 (2024).
46. L. A. Lugiato and R. Lefever, "Spatial dissipative structures in passive optical systems," Phys. Rev. Lett. **58**, 2209–2211 (1987).
47. A. Pal, A. Ghosh, S. Zhang, *et al.*, "Machine learning assisted inverse design of microresonators," Opt. Express **31**, 8020–8028 (2023).
48. Y. Li, S.-W. Huang, B. Li, *et al.*, "Real-time transition dynamics and stability of chip-scale dispersion-managed frequency microcombs," Light Sci. Appl. **9**, 52 (2020).
49. S. Fujii and T. Tanabe, "Dispersion engineering and measurement of whispering gallery mode microresonator for Kerr frequency comb generation," Nanophotonics **9**, 1087–1104 (2020).
50. A. Pal, A. Ghosh, S. Zhang, *et al.*, "Linear and nonlinear coupling of twin-resonators with Kerr nonlinearity," arXiv, arXiv:2404.05646 (2024).
51. S. A. Miller, Y. Okawachi, S. Ramelow, *et al.*, "Tunable frequency combs based on dual microring resonators," Opt. Express **23**, 21527–21540 (2015).